2011). These findings imply that catalase plays an important role in the clearance of H_2O_2 in brain tissue. H_2O_2 removal by the catalytic activity of catalase follows the pattern of a first-order reaction, and its rate relies on the H_2O_2 concentration in the environment. Given such enzymatic kinetics, catalase appears to be fully functional at removing H_2O_2 at higher concentrations. Furthermore, the contribution of catalase to the control of endogenous H_2O_2 in erythrocytes is negligible (Johnson et al., 2010). In addition, the ex vivo analysis using lung slices from wild-type (*Cat*$^{+/+}$) and *catalase* knockout mice (*Cat*$^{+/-}$ and *Cat*$^{-/-}$) revealed that the rates of H_2O_2 decomposition were proportional to the levels of catalase that were expressed, when examined at higher H_2O_2 concentrations, whereas the rates did not significantly differ among the genotypes at lower concentrations (Ho et al., 2004). Our study demonstrated that only SGCs were labeled by the oxidative damage marker, 8-OHdG, in TG. This finding is likely to reflect the inefficient H_2O_2-scavenging activity of catalase relative to GPx1 at physiologically low concentrations in SGCs. Alternatively, ROS may be actively involved in physiological signaling functions in SCGs under the normal state. Recent evidence shows that H_2O_2 functions as a second messenger by protein thiol oxidation of key proteins such as protein tyrosine phosphatases (Forman et al., 2010).

GST family members exert cytoprotective actions by catalyzing the conjugation of reactive chemicals with glutathione. Specific isoforms are known to be expressed in distinct cell populations, and GST-π is expressed primarily in oligodendrocytes in the central nervous system. The present study provides the first histological evidence that GST-π is localized in SGCs and in small- to medium-sized neurons (diameter < 35 μm) in TG. The significance of this finding is unclear. However, because GST family members are critically involved in the maintenance of the cellular antioxidant glutathione in different cellular compartments (Raza, 2011), GST-π might play a compensatory role against the absence of GPx1 in SGCs, which are equipped with less potent antioxidant machinery compared to neurons. Intriguingly, the monomeric form of GST-π is known to bind to the C-terminal of JNK and suppress its kinase activity (Wang et al., 2001). JNK activation is known to lead to the development of cell death (Shen and Liu, 2006). Although we performed the TUNEL method on TG tissue specimens, there was no evidence of apoptotic cell demise (data not shown). In spite of the evidence of oxidative damage in SGCs, they appear healthy. This enigma can be explained by the suppressive effect of GST-π on JNK activation.

TRPV1-mediated ROS production and cell death

TRPV1 activation is known to be sensitized by inflammatory mediators, such as NGF and bradykinin, via its increased expression and/or its phosphorylation, which is mediated by several kinases (Khairatkar-Joshi and Szallasi, 2009). Inflammation-mediated potentiation of the TRPV1 function is regarded as a mechanism that underlies inflammatory hyperalgesia. TRPV1 agonist stimulation of the high EGFP-flTRPV1-expressing cell line appears to mimic this situation. Under the circumstance, capsaicin treatment led to ROS-mediated caspase-3 activation. Such situations appear to be commonly encountered in meningitis and pulpitis. In addition, recent studies show that ROS are capable of augmenting TRPV1 activity by different mechanisms. NADPH oxidase-derived ROS were shown to promote protein kinase Cε (PKCε) translocation from the cytosolic to the membrane fractions, which led to TRPV1 activation by phosphorylation (Ibi et al., 2008). Moreover, covalent modification of conserved cysteines by oxidative stress results in TRPV1 sensitization (Chuang and Lin, 2009). Therefore, it is likely that inflammatory conditions favor the long-lasting enhancement of TRPV1 activation by ROS-mediated posttranslational modifications. In the present study, capsaicin treatment caused cellular demise of TRPV1-positive primary TG neurons in a dose-dependent manner, which indicates that the enhancement of TRPV1 function renders TRPV1-positive TG neurons more predisposed to cell death. Moreover, our pharmacological experiments demonstrated that the TRPV1-induced TG neuron death is mediated by ROS production and caspase activation. Although a previous study implicated ROS production in TRPV1-mediated apoptotic cell death of a nasopharyngeal carcinoma-derived cell line (Ip et al., 2012), our results provide the first evidence for the involvement of ROS in TRPV1-mediated TG neuron death. TRPV1-induced death of TG neurons does not seem to be a phenomenon restricted to an artificial *in vitro* situation because systemic capsaicin administration has been shown to induce the apoptotic cell death of primary sensory neurons in TG, DRG and nodose ganglia (Jin et al., 2005a,b; Czaja et al., 2008). Caspases constitute a family of cysteine proteases that execute apoptosis and that are implicated in a variety of neurological disease conditions, such as stroke and neurodegenerative diseases (Namura et al., 1998; Shibata et al., 2000; Yuan and Yankner, 2000; Friedlander, 2003). More specifically, caspase-3 is known to be a principal executioner caspase. Judging from the pharmacological data obtained with the high EGFP-flTRPV1-expressing cell line, ROS generation can be responsible for the caspase-3 activation. Our finding implies that the efficient elimination of ROS is likely to be a key action for rescuing primary sensory neurons from TRPV1-mediated apoptosis. What is the role of sensory neuronal death in the pathophysiology of pain disorders? Intuitively, the demise of sensory neurons appears to result in the development of sensory loss. However, there is ample evidence that loss of sensory neurons and fibers occurs in pain disorders. Diabetic neuropathic pain is recognized in approximately 10–20% of the entire diabetic population, and in 40–60% of patients with documented neuropathy (Daousi et al., 2004; Abbott et al., 2011). Diabetic neuropathy is pathologically characterized by considerable loss of small-fibers, including C- and Aδ-fibers, and oxidative stress is

postulated to play an important role in the nerve damage (Callaghan et al., 2012). Human immunodeficiency virus (HIV)-associated sensory neuropathy presents a big clinical challenge because of its increasing prevalence and its association with debilitating pain. Its viral proteins, Tat and viral protein R, are known to cause hyperexcitability of DRG neurons via excess calcium influx and impaired cyclin-dependent kinase 5 activity, which culminates in apoptosis of DRG neurons (Acharjee et al., 2010; Chi et al., 2011). Burdo et al. (2012) reported pathological features of DRG damage in simian immunodeficiency virus-infected rhesus macaques, including satellitosis, presence of Nageotte nodules, and neuronophagia as well as macrophage infiltration and abundant viral replication. Collectively, it is likely that neurodegenerative processes, which eventually lead to sensory neuronal death, can be responsible for the development of painful conditions. We surmise that the capsaicin-induced demise of TRPV1-expressing sensory neurons, which was found to be mediated by ROS production, have significant implications in the development of neuropathic pain.

Clinical implications

Our behavioral testing revealed that ROS is involved in the development of mechanical hyperalgesia in the trigeminal territory. Although mechanical hyperalgesia driven by ROS has been demonstrated in several models in rats, there seems to be controversy about the exact site of ROS production relevant to the development of mechanical hyperalgesia. Systemic and intrathecal administration of ROS scavengers showed similar efficacy against hyperalgesia induced by formalin injection and xanthine oxidase activity was elevated in the sciatic nerve in a chronic nerve constriction model, which supports peripheral ROS production (Khalil et al., 1999; Hacimuftuoglu et al., 2006). Meanwhile, some authors claim the importance of spinal involvement mainly because secondary, but not primary, capsaicin-induced hyperalgesia can be attenuated by ROS scavengers (Lee et al., 2007; Schwartz et al., 2008). As we administered the ROS scavenger, TEMPOL, intraperitoneally, we cannot determine where the agent exerted its action. Nevertheless, our cell experiments using TRPV1-expressing PC12 cell lines demonstrated the cell autonomous ROS production in response to capsaicin application and, more importantly, ROS was found to be involved in the capsaicin-induced demise of TRPV1-expressing neurons in the primary TG culture. These findings seem to lend support to the peripheral action of TEMPOL with respect to its antihyperalgesic effect.

The capsaicin-induced mechanical hyperalgesia was recognized at 2 h after capsaicin application, and face sensitivity then returned to normal levels. Such transient nature of mechanical hyperalgesia implies the presence of tight regulation of ROS levels by scavenging enzymes in the trigeminal system. Our primary culture data show that TRPV1-expressing neurons are vulnerable to capsaicin treatment in the culture condition and that capsaicin-induced TRPV1-expressing neuronal death is mediated by ROS production. Although TG neurons possess the potent antioxidant system, the culture conditions are quite different from *in vivo* situations. The cultured TG neurons are not in close contact with SGCs, and, because of the lack of elongated axons, TRPV1 stimulation occurs in the proximity to the neuronal soma. In this sense, the capsaicin stimulation in our primary culture experiments may mimic the situation in which endogenous TRPV1 agonists, such as protons and anandamide, stimulate TRPV1 in the activated state as seen in the inflammatory conditions. The trigeminal nociceptors are not infrequently involved in inflammatory disease conditions, such as meningitis, pulpitis and migraine (Moskowitz, 1984). Under these circumstances, TRPV1-mediated ROS overproduction could surpass the antioxidative capacity of trigeminal primary neurons and could contribute to compromising their viability, possibly by caspase activation. Concomitantly, the diffusion of H_2O_2 from the initially affected neurons is expected to be detrimental to the surrounding neurons. Such propagation of H_2O_2-induced neurotoxicity can be prevented by catalase, which is known to be effective at degrading H_2O_2 at higher concentrations and is located in neuron-ensheathing cells (Ho et al., 2004). In this sense, the localization of ROS-scavenging enzymes in TG is strategically important in protecting TG neurons from ROS-mediated cellular injury under the pathological conditions.

CONCLUSION

The present study has determined the cellular localization of antioxidant enzymes in TG. In terms of the decomposition of $O_2^{\cdot -}$ and peroxide, TG neurons are endowed with more potent antioxidant systems compared to SGCs. Catalase, predominantly located in SGCs, may play an important role in degrading large quantities of H_2O_2 generated in pathological conditions. We also have found that excess TRPV1 stimulation can cause toxicity to TG neurons via ROS production, which implies that therapeutic measures for antioxidative stress should be taken to prevent damage to trigeminal primary sensory neurons in inflammatory pain disorders.

Acknowledgements—This research was supported in part by a Grant-in-Aid for Scientific Research (Grant No. 22390182 to N.S.) from the Ministry of Education, Culture, Sports, Science and Technology of Japan, and a grant from the Takeda Science Foundation to M.S. There are no conflicts of interest concerning this paper.

REFERENCES

Abbott CA, Malik RA, van Ross ER, Kulkarni J, Boulton AJ (2011) Prevalence and characteristics of painful diabetic neuropathy in a large community-based diabetic population in the U.K.. Diabetes Care 34:2220–2224.

Acharjee S, Noorbakhsh F, Stemkowski PL, Olechowski C, Cohen EA, Ballanyi K, Kerr B, Pardo C, Smith PA, Power C (2010) HIV-1 viral protein R causes peripheral nervous system injury associated with in vivo neuropathic pain. FASEB J 24:4343–4353.

Amantini C, Mosca M, Nabissi M, Lucciarini R, Caprodossi S, Arcella A, Giangaspero F, Santoni G (2007) Capsaicin-induced apoptosis

of glioma cells is mediated by TRPV1 vanilloid receptor and requires p38 MAPK activation. J Neurochem 102:977–990.

Bell KF, Hardingham GE (2011) CNS peroxiredoxins and their regulation in health and disease. Antioxid Redox Signal 14:1467–1477.

Benediktsson AM, Marrs GS, Tu JC, Worley PF, Rothstein JD, Bergles DE, Dailey ME (2012) Neuronal activity regulates glutamate transporter dynamics in developing astrocytes. Glia 60:175–188.

Britsch S, Goerich DE, Riethmacher D, Peirano RI, Rossner M, Nave KA, Birchmeier C, Wegner M (2001) The transcription factor Sox10 is a key regulator of peripheral glial development. Genes Dev 15:66–78.

Burdo TH, Orzechowski K, Knight HL, Miller AD, Williams K (2012) Dorsal root ganglia damage in SIV-infected rhesus macaques: an animal model of HIV-induced sensory neuropathy. Am J Pathol 180:1362–1369.

Callaghan BC, Cheng HT, Stables CL, Smith AL, Feldman EL (2012) Diabetic neuropathy: clinical manifestations and current treatments. Lancet Neurol 11:521–534.

Camprubi-Robles M, Planells-Cases R, Ferrer-Montiel A (2009) Differential contribution of SNARE-dependent exocytosis to inflammatory potentiation of TRPV1 in nociceptors. FASEB J 23:3722–3733.

Caterina MJ, Leffler A, Malmberg AB, Martin WJ, Trafton J, Petersen-Zeitz KR, Koltzenburg M, Basbaum AI, Julius D (2000) Impaired nociception and pain sensation in mice lacking the capsaicin receptor. Science 288:306–313.

Ceruti S, Villa G, Fumagalli M, Colombo L, Magni G, Zanardelli M, Fabbretti E, Verderio C, van den Maagdenberg AM, Nistri A, Abbracchio MP (2011) Calcitonin gene-related peptide-mediated enhancement of purinergic neuron/glia communication by the algogenic factor bradykinin in mouse trigeminal ganglia from wild-type and R192Q Cav2.1 Knock-in mice: implications for basic mechanisms of migraine pain. J Neurosci 31:3638–3649.

Chi X, Amet T, Byrd D, Chang KH, Shah K, Hu N, Grantham A, Hu S, Duan J, Tao F, Nicol G, Yu Q (2011) Direct effects of HIV-1 Tat on excitability and survival of primary dorsal root ganglion neurons: possible contribution to HIV-1-associated pain. PLoS One 6:e24412.

Chuang HH, Lin S (2009) Oxidative challenges sensitize the capsaicin receptor by covalent cysteine modification. Proc Natl Acad Sci U S A 106:20097–20102.

Crack PJ, Taylor JM, Flentjar NJ, de Haan J, Hertzog P, Iannello RC, Kola I (2001) Increased infarct size and exacerbated apoptosis in the glutathione peroxidase-1 (Gpx-1) knockout mouse brain in response to ischemia/reperfusion injury. J Neurochem 78:1389–1399.

Czaja K, Burns GA, Ritter RC (2008) Capsaicin-induced neuronal death and proliferation of the primary sensory neurons located in the nodose ganglia of adult rats. Neuroscience 154:621–630.

Daousi C, MacFarlane IA, Woodward A, Nurmikko TJ, Bundred PE, Benbow SJ (2004) Chronic painful peripheral neuropathy in an urban community: a controlled comparison of people with and without diabetes. Diabet Med 21:976–982.

Davis JB, Gray J, Gunthorpe MJ, Hatcher JP, Davey PT, Overend P, Harries MH, Latcham J, Clapham C, Atkinson K, Hughes SA, Rance K, Grau E, Harper AJ, Pugh PL, Rogers DC, Bingham S, Randall A, Sheardown SA (2000) Vanilloid receptor-1 is essential for inflammatory thermal hyperalgesia. Nature 405:183–187.

Dringen R, Pawlowski PG, Hirrlinger J (2005) Peroxide detoxification by brain cells. J Neurosci Res 79:157–165.

Flentjar NJ, Crack PJ, Boyd R, Malin M, de Haan JB, Hertzog P, Kola I, Iannello R (2002) Mice lacking glutathione peroxidase-1 activity show increased TUNEL staining and an accelerated inflammatory response in brain following a cold-induced injury. Exp Neurol 177:9–20.

Forman HJ, Maiorino M, Ursini F (2010) Signaling functions of reactive oxygen species. Biochemistry 49:835–842.

Franklin JL (2011) Redox regulation of the intrinsic pathway in neuronal apoptosis. Antioxid Redox Signal 14:1437–1448.

Friedlander RM (2003) Apoptosis and caspases in neurodegenerative diseases. N Engl J Med 348:1365–1375.

Hacimuftuoglu A, Handy CR, Goettl VM, Lin CG, Dane S, Stephens Jr RL (2006) Antioxidants attenuate multiple phases of formalin-induced nociceptive response in mice. Behav Brain Res 173:211–216.

Hanani M (2010) Satellite glial cells: more than just 'rings around the neuron'. Neuron Glia Biol 6:1–2.

Ho YS, Xiong Y, Ma W, Spector A, Ho DS (2004) Mice lacking catalase develop normally but show differential sensitivity to oxidant tissue injury. J Biol Chem 279:32804–32812.

Honda K, Kitagawa J, Sessle BJ, Kondo M, Tsuboi Y, Yonehara Y, Iwata K (2008) Mechanisms involved in an increment of multimodal excitability of medullary and upper cervical dorsal horn neurons following cutaneous capsaicin treatment. Mol Pain 4:59.

Ibi M, Matsuno K, Shiba D, Katsuyama M, Iwata K, Kakehi T, Nakagawa T, Sango K, Shirai Y, Yokoyama T, Kaneko S, Saito N, Yabe-Nishimura C (2008) Reactive oxygen species derived from NOX1/NADPH oxidase enhance inflammatory pain. J Neurosci 28:9486–9494.

Ip SW, Lan SH, Lu HF, Huang AC, Yang JS, Lin JP, Huang HY, Lien JC, Ho CC, Chiu CF, Wood W, Chung JG (2012) Capsaicin mediates apoptosis in human nasopharyngeal carcinoma NPC-TW 039 cells through mitochondrial depolarization and endoplasmic reticulum stress. Hum Exp Toxicol 31:539–549.

Jin HW, Ichikawa H, Fujita M, Yamaai T, Mukae K, Nomura K, Sugimoto T (2005a) Involvement of caspase cascade in capsaicin-induced apoptosis of dorsal root ganglion neurons. Brain Res 1056:139–144.

Jin HW, Ichikawa H, Nomura K, Mukae K, Terayama R, Yamaai T, Sugimoto T (2005b) Activation of the caspase cascade underlies the rat trigeminal primary neuronal apoptosis induced by neonatal capsaicin administration. Arch Histol Cytol 68:301–310.

Johnson RM, Ho YS, Yu DY, Kuypers FA, Ravindranath Y, Goyette GW (2010) The effects of disruption of genes for peroxiredoxin-2, glutathione peroxidase-1, and catalase on erythrocyte oxidative metabolism. Free Radic Biol Med 48:519–525.

Katagiri A, Shinoda M, Honda K, Toyofuku A, Sessle BJ, Iwata K (2012) Satellite glial cell P2Y12 receptor in the trigeminal ganglion is involved in lingual neuropathic pain mechanisms in rats. Mol Pain 8:23.

Khairatkar-Joshi N, Szallasi A (2009) TRPV1 antagonists: the challenges for therapeutic targeting. Trends Mol Med 15: 14–22.

Khalil Z, Liu T, Helme RD (1999) Free radicals contribute to the reduction in peripheral vascular responses and the maintenance of thermal hyperalgesia in rats with chronic constriction injury. Pain 79:31–37.

Kim HK, Park SK, Zhou JL, Taglialatela G, Chung K, Coggeshall RE, Chung JM (2004) Reactive oxygen species (ROS) play an important role in a rat model of neuropathic pain. Pain 111:116–124.

Kim HK, Zhang YP, Gwak YS, Abdi S (2010) Phenyl N-tert-butylnitrone, a free radical scavenger, reduces mechanical allodynia in chemotherapy-induced neuropathic pain in rats. Anesthesiology 112:432–439.

Kuhad A, Sharma S, Chopra K (2008) Lycopene attenuates thermal hyperalgesia in a diabetic mouse model of neuropathic pain. Eur J Pain 12:624–632.

Lee I, Kim HK, Kim JH, Chung K, Chung JM (2007) The role of reactive oxygen species in capsaicin-induced mechanical hyperalgesia and in the activities of dorsal horn neurons. Pain 133:9–17.

Mao YF, Yan N, Xu H, Sun JH, Xiong YC, Deng XM (2009) Edaravone, a free radical scavenger, is effective on neuropathic pain in rats. Brain Res 1248:68–75.

Marin-Valencia I, Good LB, Ma Q, Duarte J, Bottiglieri T, Sinton CM, Heilig CW, Pascual JM (2012) Glut1 deficiency (G1D): epilepsy and metabolic dysfunction in a mouse model of the most common human phenotype. Neurobiol Dis 48:92–101.

Maro GS, Vermeren M, Voiculescu O, Melton L, Cohen J, Charnay P, Topilko P (2004) Neural crest boundary cap cells constitute a source of neuronal and glial cells of the PNS. Nat Neurosci 7:930–938.

McCommis KS, McGee AM, Laughlin MH, Bowles DK, Baines CP (2011) Hypercholesterolemia increases mitochondrial oxidative stress and enhances the MPT response in the porcine myocardium: beneficial effects of chronic exercise. Am J Physiol Regul Integr Comp Physiol 301: R1250–R1258.

McCubrey JA, Lahair MM, Franklin RA (2006) Reactive oxygen species-induced activation of the MAP kinase signaling pathways. Antioxid Redox Signal 8:1775–1789.

Mika J, Osikowicz M, Makuch W, Przewlocka B (2007) Minocycline and pentoxifylline attenuate allodynia and hyperalgesia and potentiate the effects of morphine in rat and mouse models of neuropathic pain. Eur J Pharmacol 560:142–149.

Mitozo PA, de Souza LF, Loch-Neckel G, Flesch S, Maris AF, Figueiredo CP, Dos Santos AR, Farina M, Dafre AL (2011) A study of the relative importance of the peroxiredoxin-, catalase-, and glutathione-dependent systems in neural peroxide metabolism. Free Radic Biol Med 51:69–77.

Moskowitz MA (1984) The neurobiology of vascular head pain. Ann Neurol 16:157–168.

Nagai T, Ibata K, Park ES, Kubota M, Mikoshiba K, Miyawaki A (2002) A variant of yellow fluorescent protein with fast and efficient maturation for cell-biological applications. Nat Biotechnol 20:87–90.

Namura S, Zhu J, Fink K, Endres M, Srinivasan A, Tomaselli KJ, Yuan J, Moskowitz MA (1998) Activation and cleavage of caspase-3 in apoptosis induced by experimental cerebral ischemia. J Neurosci 18:3659–3668.

Patenaude A, Murthy MR, Mirault ME (2005) Emerging roles of thioredoxin cycle enzymes in the central nervous system. Cell Mol Life Sci 62:1063–1080.

Power JH, Blumbergs PC (2009) Cellular glutathione peroxidase in human brain: cellular distribution, and its potential role in the degradation of Lewy bodies in Parkinson's disease and dementia with Lewy bodies. Acta Neuropathol 117:63–73.

Rappaport ZH, Devor M (1994) Trigeminal neuralgia: the role of self-sustaining discharge in the trigeminal ganglion. Pain 56:127–138.

Raza H (2011) Dual localization of glutathione S-transferase in the cytosol and mitochondria: implications in oxidative stress, toxicity and disease. FEBS J 278:4243–4251.

Salvemini D, Little JW, Doyle T, Neumann WL (2011) Roles of reactive oxygen and nitrogen species in pain. Free Radic Biol Med 51:951–966.

Schwartz ES, Lee I, Chung K, Chung JM (2008) Oxidative stress in the spinal cord is an important contributor in capsaicin-induced mechanical secondary hyperalgesia in mice. Pain 138:514–524.

Shen HM, Liu ZG (2006) JNK signaling pathway is a key modulator in cell death mediated by reactive oxygen and nitrogen species. Free Radic Biol Med 40:928–939.

Shibata M, Hisahara S, Hara H, Yamawaki T, Fukuuchi Y, Yuan J, Okano H, Miura M (2000) Caspases determine the vulnerability of oligodendrocytes in the ischemic brain. J Clin Invest 106:643–653.

Shibata S, Yasuda A, Renault-Mihara F, Suyama S, Katoh H, Inoue T, Inoue YU, Nagoshi N, Sato M, Nakamura M, Akazawa C, Okano H (2010) Sox10-Venus mice: a new tool for real-time labeling of neural crest lineage cells and oligodendrocytes. Mol Brain 3:31.

Shin CY, Shin J, Kim BM, Wang MH, Jang JH, Surh YJ, Oh U (2003) Essential role of mitochondrial permeability transition in vanilloid receptor 1-dependent cell death of sensory neurons. Mol Cell Neurosci 24:57–68.

Takeda M, Takahashi M, Matsumoto S (2009) Contribution of the activation of satellite glia in sensory ganglia to pathological pain. Neurosci Biobehav Rev 33:784–792.

Thiemermann C (2003) Membrane-permeable radical scavengers (tempol) for shock, ischemia–reperfusion injury, and inflammation. Crit Care Med 31:S76–84.

Tominaga M, Caterina MJ, Malmberg AB, Rosen TA, Gilbert H, Skinner K, Raumann BE, Basbaum AI, Julius D (1998) The cloned capsaicin receptor integrates multiple pain-producing stimuli. Neuron 21:531–543.

Toyokuni S, Tanaka T, Hattori Y, Nishiyama Y, Yoshida A, Uchida K, Hiai H, Ochi H, Osawa T (1997) Quantitative immunohistochemical determination of 8-hydroxy-2′-deoxyguanosine by a monoclonal antibody N45.1: its application to ferric nitrilotriacetate-induced renal carcinogenesis model. Lab Invest 76:365–374.

Wang T, Arifoglu P, Ronai Z, Tew KD (2001) Glutathione S-transferase P1-1 (GSTP1-1) inhibits c-Jun N-terminal kinase (JNK1) signaling through interaction with the C terminus. J Biol Chem 276:20999–21003.

Yowtak J, Lee KY, Kim HY, Wang J, Kim HK, Chung K, Chung JM (2011) Reactive oxygen species contribute to neuropathic pain by reducing spinal GABA release. Pain 152:844–852.

Yuan J, Yankner BA (2000) Apoptosis in the nervous system. Nature 407:802–809.

Zhang J, Graham DG, Montine TJ, Ho YS (2000) Enhanced N-methyl-4-phenyl-1,2,3,6-tetrahydropyridine toxicity in mice deficient in CuZn-superoxide dismutase or glutathione peroxidase. J Neuropathol Exp Neurol 59:53–61.

(Accepted 1 June 2013)
(Available online 15 June 2013)

Journal of Neuroscience Research

Journal of Neuroscience Research 91:578–584 (2013)

Potassium-Induced Cortical Spreading Depression Bilaterally Suppresses the Electroencephalogram but Only Ipsilaterally Affects Red Blood Cell Velocity in Intraparenchymal Capillaries

Miyuki Unekawa,[1]* Yutaka Tomita,[1] Haruki Toriumi,[1] Kazuto Masamoto,[2,3] Iwao Kanno,[3] and Norihiro Suzuki[1]

[1]Department of Neurology, School of Medicine, Keio University, Tokyo, Japan
[2]Center for Frontier Science and Engineering, University of Electro-Communications, Tokyo, Japan
[3]Molecular Imaging Center, National Institute of Radiological Sciences, Chiba, Japan

Cortical spreading depression (CSD) is a repetitive, propagating profile of mass depolarization of neuronal and glial cells, followed by sustained suppression of spontaneous neuronal activity. We have reported a long-lasting suppressive effect on red blood cell (RBC) velocities in intraparenchymal capillaries. Here, to test the hypothesis that the prolonged decrease of RBC velocity in capillaries is due to suppression of neuronal activity, we measured CSD-elicited changes in the electroencephalogram (EEG) as an index of neuronal activity. In isoflurane-anesthetized rats, DC potential, EEG, partial pressure of oxygen (PO_2), and cerebral blood flow (CBF) were simultaneously recorded in the temporo-parietal region. The velocities of fluorescently labeled RBCs were evaluated by high-speed camera laser scanning confocal fluorescence microscopy with our original software, KEIO-IS2. Transient deflection of DC potential and PO_2 and increase of CBF were repeatedly detected only in the ipsilateral hemisphere following topical KCl application. On the other hand, the relative spectral power of EEG was reduced bilaterally, showing the lowest value at 5 min after KCl application, when the other parameters had already returned to the baseline after the passage of CSD. Mean RBC velocity in capillaries was slightly but significantly reduced during and after passage of CSD in the ipsilateral hemisphere but did not change in the contralateral hemisphere in the same rats. We suggest that mass depolarization of neuronal and glial cells might transiently decelerate RBCs in nearby capillaries, but the sustained reduction of ipsilateral RBC velocity might be a result of the prolonged effect of CSD, not of neuronal suppression alone.

Key words: cortical spreading depression; cerebral microcirculation; electroencephalogram; transhemispheric projection; RBC velocity

Cortical spreading depression (CSD) is a repetitive mass depolarization of neuronal and glial cells, followed by a sustained suppression of spontaneous neuronal activity (Leão, 1944). CSD is involved in the mechanism of migraine aura, which starts in the primary visual cortex and moves toward the periphery at the rate of approximately 3 mm/min (Lauritzen, 2001). At the beginning of migraine attacks, cerebral blood flow (CBF) decreases in the posterior part of the brain, and then the hypoperfusion spreads into the parietal and temporal lobes at the rate of 2–3 mm/min for 30–60 min (so-called spreading oligemia; Olesen et al., 1981). In an experimental model, artificially evoked CSD elicited a rise of CBF, followed by a long-lasting reduction to below the prestimulus level (Lauritzen et al., 1982; Kocher, 1990; Fabricius and Lauritzen, 1993).

It has been accepted that CSD does not propagate from one hemisphere to the other and does not interfere with the circulation or cause edema in the contralateral cortex (Bueš et al., 1974). The side of the headache usually corresponds to the side of the vascular changes (Olesen et al., 1990). On the other hand, CSD induced by fine-needle stab or topical application of tetrodotoxin (TTX) elicited a pronounced decrease of the spontaneous spike rate in layers III through IV of the contralateral cortex (Enager et al., 2004). Electrical stimulation of transcallosal fibers produces electrophysiologic and

Contract grant sponsor: Ministry of Education, Culture, Sports, Science and Technology of Japan; Contract grant number: 22390182 (to N.S.); Contract grant number: 24500422 (to Y.T.); Contract grant sponsor: Otsuka Pharmaceutical Co., Ltd.

*Correspondence to: Miyuki Unekawa, Department of Neurology, School of Medicine, Keio University, 35 Shinanomachi, Shinjuku-ku, Tokyo 160-8582, Japan. E-mail: unekawa.m@z5.keio.jp

Received 27 June 2012; Revised 10 October 2012; Accepted 10 November 2012

Published online 18 January 2013 in Wiley Online Library (wileyonlinelibrary.com). DOI: 10.1002/jnr.23184

hemodynamic responses in contralateral cortical regions via neuronal transmission (Hoffmeyer et al., 2007). Furthermore, stimulation of the hindpaw motor cortex evoked a bilateral blood oxygenation level-dependent fMRI signal via corticocortical pathways (Austin et al., 2003). Mono- and polysynaptic connections, including callosal cells, are involved in interhemisphere interactions (Bogdanova and Sil'kis, 1999). Thus, it is likely that unilateral elicitation of CSD would affect neuronal activity in the contralateral hemisphere.

Recently, the concept of the neurovascular unit, in which neurons and microvessels appear to communicate with each other, with the participation of the intervening astrocytes, has been proposed and investigated (del Zoppo, 2010). Namely, neuronal activity and microcirculation in the adjacent area are closely interlinked. Red blood cell (RBC) behavior in capillaries is especially important, because RBCs are the predominant oxygen carrier from the lung to the tissue. We have found that RBC velocity in intraparenchymal capillaries is often independent of upstream arteriolar blood flow or tissue perfusion in the surrounding microvasculature; for example, RBC velocity in capillaries remained unchanged in response to topical application of nitroprusside on the brain surface in spite of a dramatic increase in local CBF (Tomita et al., 2009).

We have developed a method for measurement of the velocity of individual RBCs in capillaries *in vivo*, using a high-speed camera laser scanning confocal fluorescence microscope system with Matlab-domain analysis software, KEIO-IS2 (Schiszler et al., 2005; Tomita et al., 2008; Unekawa et al., 2008). We observed heterogeneous changes of RBC velocity in capillaries, namely, both a sustained decrease and a remarkable increase, after KCl application on the cerebral cortex, while CBF as measured by laser Doppler flowmetry was elevated (Unekawa et al., 2012). In that study, the number of slowed RBCs was dramatically increased during CSD, and a similar tendency was seen even after passage of CSD, in spite of the recovery of DC potential, partial pressure of oxygen (PO_2), and CBF.

In the course of our study, we noticed that the electroencephalogram (EEG), reflecting spontaneous neuronal activity was bilaterally suppressed even after the passage of CSD. We speculated that the prolonged decrease of RBC velocity was due to this suppression of neuronal activity. To examine this hypothesis, we simultaneously evaluated the transhemispheric effects on spontaneous neuronal activity and on RBC velocity in intraparencymal capillaries in response to potassium-induced CSD in the same animal. We discuss the relationship between neuronal activity and RBC flow in single capillaries.

MATERIALS AND METHODS

General Procedures

Animals were used with the approval (No. 09058) of the Animal Ethics Committee of Keio University (Tokyo, Japan), and all experimental procedures were in accordance with the university's guidelines for the care and use of laboratory animals. General procedures were as described in our previous article (Unekawa et al., 2012). Male Sprague-Dawley rats (CLEA Japan, Inc., Tokyo, Japan; 10–15 weeks, body weight 411 ± 134 g, n = 17) were anesthetized with isoflurane (2.5–3.0% in room air, with a flow rate of 250 ml/min) via a concentration-controllable anesthesia unit (model 400; Univentor Ltd., Zejtun, Malta). Arterial blood pressure (ABP) was continuously recorded through a femoral arterial catheter via a surgical strain-gauge (MLT0670 and ML117; ADInstruments Pty. Ltd., Bella Vista, New South Wales, Australia), and heart rate (HR) was determined from the ABP wave. Body temperature was maintained with a heating pad and thermocontroller (BWT-100; Bioresearch Center Co., Ltd., Nagoya, Japan).

Study of Transhemispheric Effects

Measurements of PO_2, CBF, and DC potential were made as described in our previous article (Unekawa et al., 2012). Each rat was fixed to a head-holder (SG-3N, modified to be flexible around the horizontal axis; Narishige Scientific Instrument Laboratory, Tokyo, Japan), and two windows of approximately 3 mm width were made bilaterally at the parieto-temporal region of the cerebral cortex. As shown in Figure 1A,B (n = 7), an electrode for measuring PO_2 (POE-10N; Bioresearch Center Co., Ltd.), an electrode for DC potential (EEG-5002Ag; Bioresearch Center Co., Ltd.), and the probe of a laser Doppler flowmeter (ALF 21R; Advance Co., Ltd., Tokyo, Japan) were positioned at the right window, and another electrode for DC potential was positioned at the left window, after removal of the dura. These electrodes and probe were fixed in place and sealed with dental cement to prevent the brain surface from drying. Reference electrodes for PO_2 (POR-10N; Bioresearch Center Co., Ltd.) and DC potential (EER-5004Ag; Bioresearch Center Co., Ltd.) were placed subcutaneously in the back and under the scalp, respectively. PO_2 was continuously monitored with an oxygen monitor (PO2-100DW; Inter Medical Co., Ltd., Nagoya, Japan). The DC potential was amplified at 1–100 Hz with a sampling rate of 1 kHz using a differential headstage and a differential extracellular amplifier (models 4002 and EX1; Dagan Co., Minneapolis, MN). Continuous recordings of ABP as well as HR, PO_2, CBF, and DC potential were stored on a multichannel recorder (PowerLab 8/30; ADInstruments Pty Ltd.) and evaluated with off-line analysis software (LabChart; ADInstruments Pty Ltd.). EEG was obtained by digital filtering of the DC potential signal with a 5-Hz low cut, to minimize basal fluctuations resulting from heart rate and breathing. The EEG signal was calculated by fast Fourier frequency analysis every 1 min, and the maximum value at each frequency was employed to determine EEG spectral power. The peak value was found at the frequency of about 8–11 Hz, namely, α-wave, in all rats. PO_2, CBF, and DC potential were averaged for every 10 sec. KCl solution (1.0 M, 5 μl) was applied into a posterior hole on either side having a center at the coordinates of 7 mm posterior and 2 mm lateral to bregma, after confirmation that all parameters had remained stable for at least 10 min, and a further application was made into the

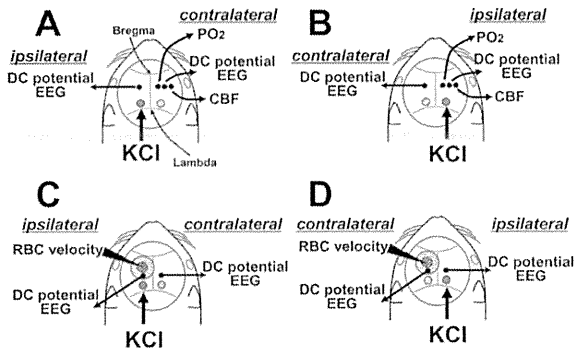

Fig. 1. Positioning of electrodes for DC potential, an electrode for PO_2, and a laser Doppler flowmeter probe in the cranial window for transhemispheric study (**A,B**) and RBC velocity study (**C,D**). EEG was calculated from the DC potential signal as mentioned in Materials and Methods. When KCl was applied to the left hole, contralateral DC potential, PO_2, and CBF were recorded in parallel with ipsilateral DC potential (A). When KCl was applied to the right hole, ipsilateral DC potential, PO_2, and CBF were recorded in parallel with contralateral DC potential (B) in the same rat. Ipsilateral or contralateral confocal movies were obtained in the shaded area to measure RBC velocity before and after application of KCl to the left (C) or the right (D) hole, respectively.

posterior hole on the other side at least 30 min after the last CSD, when all parameters including EEG had recovered. KCl application at the concentration used here elicited several CSD episodes within a 20-min interval without exception, but analysis of EEG and other parameters was performed during the first CSD episode to avoid the influence of the previous episode(s).

Analysis of RBC Velocity

Measurement of RBC velocity was conducted as described previously (Tomita et al., 2008; Unekawa et al., 2008). A cranial window of approximately 4 mm diameter was made at the left parietotemporal region of the cerebral cortex. As shown in Figure 1C,D (n = 10), DC potential electrodes were fixed at the posterior edge of the left window and at the symmetric position across the sagittal suture on the contralateral side. KCl solution (1.0 M, 5 μl) was applied alternately into the additional posterior holes on both sides, having a center at the coordinates of 7 mm posterior and 2 mm lateral to bregma. An appropriate capillary-rich area around the center of the cranial window was selected, and 0.5 ml of fluorescein isothiocyanate (FITC)-labeled RBC suspension, prepared beforehand according to Seylaz et al. (1999), was injected into the bloodstream so that the final percentage of FITC-labeled RBCs/total RBCs in the circulating blood was approximately 0.4%. The velocities of individual FITC-labeled RBCs were automatically calculated using a high-speed camera (500 fps) laser scanning confocal fluorescence microscope and an image analysis system in the Matlab (The MathWorks, Natick, MA) environment with application software (KEIO-IS2) developed in our laboratory (Schiszler et al., 2005; Tomita et al., 2008). Motion images were obtained at the depth of approximately 80 μm from the brain surface (layer I of the cerebral cortex) and analyzed in an area of 600 × 400 μm. The images acquired with the high-speed system could be recorded for up to 15 sec because of the limitation of file size (2 GB) in our analysis system. With reference to alternatively recorded images obtained using a conventional video camera, we defined single capillaries as having a diameter of less than 10 μm, based on other reports (Williams et al., 1993; Hutchinson et al., 2006). The frequency distribution of RBC velocity was obtained by classification of velocities in steps of 0.5 mm/sec and counting the RBCs within each step. RBC appearance was represented as a percentage of the total number of detected RBCs.

Statistical Analysis

All data are reported as mean ± SD. Statistical analysis of transhemispheric effects was performed via Student's *t*-test after Levene's test for equality of variance. Statistical analysis of EEG spectral power was performed with paired parametric multiple comparison (Bonferroni's test) after demonstration of homogeneity with repeated-measures ANOVA (Friedman's test). Statistical analysis of frequency distribution of RBC velocity was performed with nonparametric multiple comparisons (Bonferroni's test) after demonstration of homogeneity of variance with one-way ANOVA (Kruskal Wallis test). $P < 0.05$ was considered statistically significant.

RESULTS

General Results

Initial levels of mean ABP (MABP) and HR were 75 ± 6 mmHg and 327 ± 49 bpm, respectively. MABP and HR were maintained within ±20 mmHg and ±50 bpm in each rat throughout the experiments. MABP did not decrease below 60 mmHg in any rat. Average MABP and HR were 72 ± 12 mmHg and 314 ± 51 bpm at the end of the experiment.

Transhemispheric Effect of CSD

When KCl was applied to the left side, as shown in Figure 1A, DC potential, PO_2, and CBF of the right (contralateral) side did not change, whereas DC potential deflection was seen on the left (ipsilateral) side (Fig. 2A). In the same rat, when KCl was applied to the right side, as shown in Figure 1B, DC potential, PO_2, and CBF on the right (ipsilateral) side showed a specific response as described previously (Unekawa et al., 2012), without DC potential deflection at the left (contralateral) side, as shown in Figure 2B. Namely, potassium-induced responses of DC potential, PO_2, and CBF propagated only within the same hemisphere. On the other hand, EEG was bilaterally suppressed for a longer time. ABP was constant independently of the site of KCl application; that is, the responses were locally elicited and were not due to a change in systemic BP.

Average changes of DC potential, PO_2, CBF, and EEG spectral power on the ipsilateral and contralateral sides after KCl application are plotted in Figure 3. DC potential deflection, transient decrease in PO_2, and

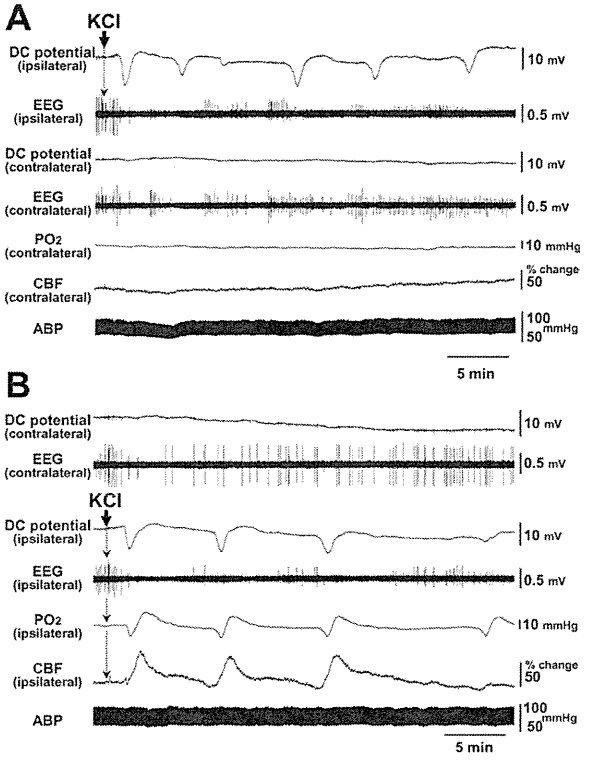

Fig. 2. Sample recordings of DC potential, EEG, PO_2, CBF, and ABP in response to KCl application. **A:** Response to KCl application on the left side, as shown in Figure 1A. **B:** Response to KCl application on the right side, as shown in Figure 1B in the same rat.

increase in CBF were observed on the ipsilateral side (Fig. 3A). However, these parameters did not change at all on the contralateral side (Fig. 3B). On the other hand, EEG spectral power was reduced in a sustained manner on both sides after unilateral application of KCl, showing a trough at 5 min after KCl application, when the other parameters had recovered to their base levels. The suppressive response on the ipsilateral side was statistically significantly larger than that on the contralateral side (Fig. 3C).

Change of RBC Velocity in Capillaries

As shown in Figure 4A, confocal microscopic movies for the analysis of RBC velocity were recorded for 10–15 sec at representative periods, i.e., before KCl application (Before-KCl), just after the trough of the DC potential at the ipsilateral side (Intra-CSD), between CSD when all parameters had returned to the baseline (Inter-CSD), and approximately 1 hr after KCl application when CSD had ceased (After-CSD), in the same manner as in the previous report (Unekawa et al., 2012).

RBC appearance (frequency distribution of RBC velocity in capillaries) showed a peak in the range of 1.0–1.5 mm/sec, with tailing to higher velocities of up to 8.6 mm/sec (Fig. 4B,C; see Before-KCl), which is broadly consistent with our previous findings (Unekawa et al., 2008). After ipsilateral application of KCl, the peak was shifted to the range of 0.5–1.0 mm/sec, namely, to slower velocity (Fig. 4B). This tendency was more apparent at Intra-CSD than at Inter-CSD, again in agreement with our previous report (Unekawa et al., 2012). Mean RBC velocity in single capillaries after ipsilateral application of KCl was statistically significantly decreased to 1.48 ± 1.18 mm/sec (for 337 detected RBCs) at Intra-CSD from the level of Before-KCl (1.74 ± 1.35 mm/sec for 527 detected RBCs), as shown in Figure 4B (inset). The mean velocity was further decreased to 1.34 ± 0.94 mm/sec (for 291 detected RBCs) at Inter-CSD and 1.31 ± 0.72 mm/sec (for 239 detected RBCs) at After-CSD. On the other hand, contralateral application of KCl did not affect the frequency distribution at any recording period (Fig. 4C). The mean velocity after contralateral application of KCl in the same rat was unchanged throughout the serial recording period (Before-KCl, 1.72 ± 1.05 mm/sec for 1,047 detected RBCs; Intra-CSD, 1.68 ± 1.11 mm/sec for 1,406 detected RBCs; Inter-CSD, 1.72 ± 1.14 mm/s for 1,005 detected RBCs; After-CSD, 1.68 ± 1.34 mm/sec for 593 detected RBCs), as shown in Figure 4C (inset).

DISCUSSION

The occurrence of propagating unilateral CSD within the ipsilateral hemisphere (Bueš et al., 1974) has been generally accepted. Nevertheless, our findings that the typical CSD-induced changes in DC potential, PO_2, and CBF did not propagate to the contralateral hemisphere serve to strengthen this idea and define the transhemispherical profile more precisely than before (Mayevsky and Weiss, 1991; Back et al., 1994), because all the parameters were continuously and simultaneously recorded and were repeatedly observed in the same animal.

On the other hand, we observed a sustained and bilateral suppression of EEG spectral power in this experiment. Although administration of narcotics alters the peak frequency obtained from power spectral analysis, the frequency domain of EEG signals was relatively constant in anesthetized rats (Chang et al., 1995). The peak frequency obtained in our experiment was limited to the α component range, suggesting that the CSD-induced EEG suppression may be a general neuronal depression rather than an effect on a specific mechanism.

Reduced spontaneous neuronal activity induced by the CSD in the contralateral hemisphere may be related to the phenomenon of diaschisis. Neuronal deactivation in the cerebral cortex by cerebral artery occlusion, topical application of TTX or needle stab-induced CSD reduced blood flow, EEG, and neuronal spontaneous spike rates in the bilateral cerebellar cortex (Gold and Lauritzen, 2002). Furthermore, unilateral application of TTX or CSD reduced cortical spontaneous spike rates in the contralateral sensory cortex (Enager et al., 2004).

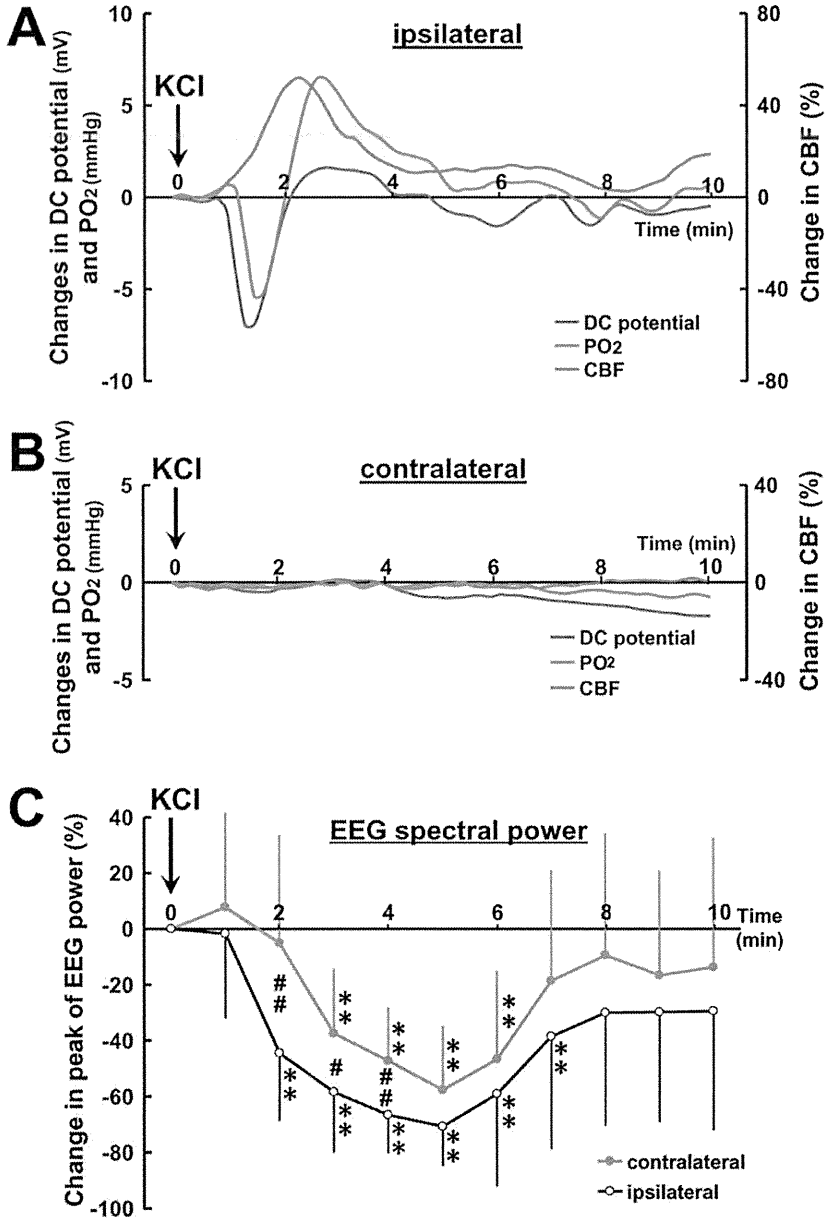

Fig. 3. Average response curves of DC potential, PO_2, CBF, and EEG peak spectral power on the ipsilateral and contralateral sides. Average changes of DC potential (blue), PO_2 (red), and CBF (green) from the level before KCl application for every 10 sec after KCl application are shown for the ipsilateral side (**A**) and the contralateral side (**B**). **C:** Time course of peak EEG spectral power averaged for every 1 min in response to ipsilateral application (open circles) and contralateral application (solid circles) of KCl. $^{**}P < 0.01$ significant difference from the level before KCl application. $^{\#}P < 0.05$, $^{\#\#}P < 0.01$ significant difference between ipsilateral and contralateral sides.

The time course of bilateral suppression of the spike rate was very similar to that of suppression of the EEG spectral power observed in our experiment, so we consider that EEG spectral power reflects the status of spontaneous neuronal activity in the contralateral hemisphere.

Transhemispherical transmission of neuronal activity seems to be mediated via transhemipheric neuronal projections such as corpus callosum (Conti and Manzoni, 1994; Bogdanova and Sil'kis, 1999). This idea is supported by the results showing that electrical stimulation of transcallosal fibers elicited a biphasic postsynaptic potential response, including initial negative potential change (excitation) and following long-lasting positive potential change (inhibition), accompanied by CBF increase (Hoffmeyer et al., 2007). Thus, decrease of excitatory input and/or increase of inhibitory input via

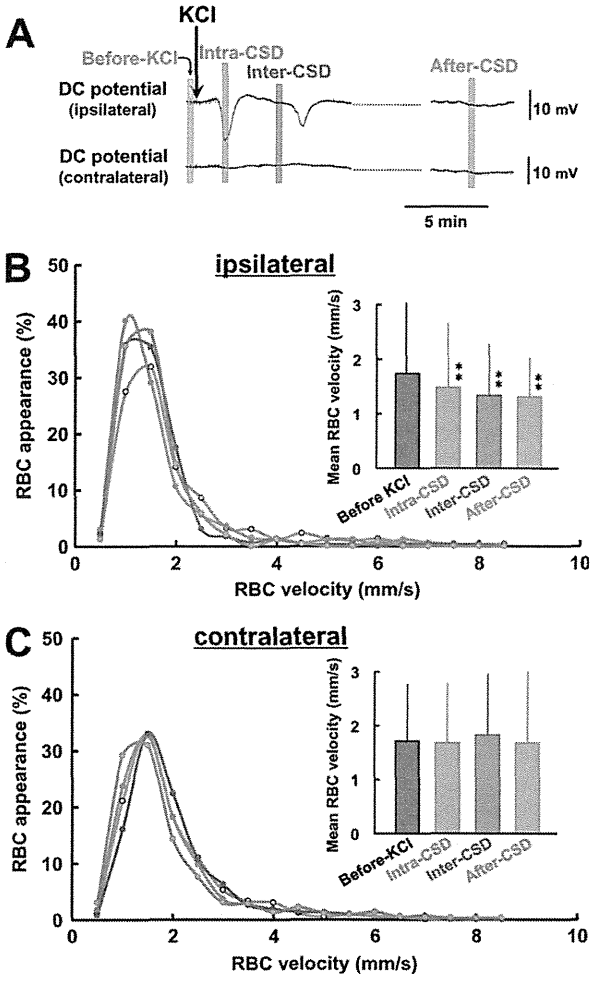

Fig. 4. Summary of RBC velocities in single capillaries. Motion pictures were obtained with the high-speed camera laser scanning confocal microscope at the timings shown in **A**; before KCl application (Before-KCl; gray), just after the trough of DC potential deflection (Intra-CSD; red), several minutes after the DC potential had recovered (Inter-CSD; blue), and 1 hr after KCl application (After-CSD; green). Frequency distribution of RBC velocities in capillaries before and after ipsilateral (**B**) and contralateral (**C**) application of KCl. Average velocities of total detected RBCs are shown in the **insets**. $^{**}P < 0.01$ significant difference from Before-KCl.

interhemispheric projections caused by unilateral CSD might suppress neuronal activity and affect the microcirculation in the contralateral hemisphere.

There have been conflicting reports regarding the response of capillary flow to potassium-induced CSD in the ipsilateral hemisphere, such as an increase of flow concurrently with arterial dilation followed by a relative decrease during oligemia in adult mice (Takano et al., 2007), a fall with an occasional transient cessation in neonatal rats (Chuquet et al., 2007), a transient decrease with occasional full stop in adult rats (Tomita et al., 2005, 2011), and a heterogeneous profile with a long-lasting decrease and a remarkable increase in adult rats (Unekawa et al., 2012). In addition to CSD-induced vasoconstriction following vasodilation of parenchymal arterioles (Osada et al., 2006), neuronal swelling (Takano et al., 2007; Zhou et al., 2010), morphological changes of astrocytes (Tomita et al., 2011), and capillary constriction by oxidative-nitrative stress-induced pericyte contraction (Yemisci et al., 2009) have been described. Thus, capillary resistance might be altered through some physical and/or hemorheological mechanism(s), such as alteration of shear stress and/or hemodilution in nearby capillaries (Hudetz, 1997), increase of plasma viscosity (Tomita et al., 2011), or swelling of endothelial cells, as seen under ischemia/reperfusion (Itoh and Suzuki, 2012). Our present results suggest that sustained neuronal depression alone might be too small to elicit apparent changes in RBC velocity as well as metabolism and local CBF.

CONCLUSIONS

Unilateral application of KCl on the surface of the cerebral cortex induced a short-lasting DC potential deflection with a long-lasting suppression of RBC velocity only in the ipsilateral hemisphere, with neither a typical CSD response nor an RBC velocity change in the contralateral hemisphere. Nevertheless, a significant, long-lasting suppression of EEG spectral power following the CSD events was found in both hemispheres. These findings suggest that CSD-induced changes in RBC velocity in single capillaries might be elicited by mass depolarization of neurons and glial cells in their vicinity, but not by a long-lasting suppression of spontaneous neuronal activity.

ACKNOWLEDGMENTS

The authors declare that they have no conflicts of interest.

REFERENCES

Austin VC, Blamire AM, Grieve SM, O'Neill MJ, Styles P, Matthews PM, Sibson NR. 2003. Differences in the BOLD fMRI response to direct and indirect cortical stimulation in the rat. Magn Reson Med 49:838–847.

Back T, Kohno K, Hossmann KA. 1994. Cortical negative DC deflections following middle cerebral artery occlusion and KCl-induced spreading depression: effect on blood flow, tissue oxygenation, and electroencephalogram. J Cereb Blood Flow Metab 14:12–19.

Bogdanova OG, Sil'kis IG. 1999. The effects of high-frequency microstimulation of the cortex on interhemisphere synchronization in the rat motor cortex. Neurosci Behav Physiol 29:515–522.

Bueš J, Burešová O, Køivánek J. 1974. The mechanism and applications of Leão's spreading depression of electroencephalographic activity. Prague: Academia.

Chang AY, Kuo TB, Tsai TH, Chen CF, Chan SH. 1995. Power spectral analysis of electroencephalographic desynchronization induced by cocaine in rats: correlation with evaluation of noradrenergic neurotransmission at the medial prefrontal cortex. Synapse 21:149–157.

Chuquet J, Hollender L, Nimchinsky EA. 2007. High-resolution in vivo imaging of the neurovascular unit during spreading depression. J Neurosci 27:4036–4044.

Conti F, Manzoni T. 1994. The neurotransmitters and postsynaptic actions of callosally projecting neurons. Behav Brain Res 64:37–53.

del Zoppo GJ. 2010. The neurovascular unit in the setting of stroke. J Intern Med 267:156–171.

Enager P, Gold L, Lauritzen M. 2004. Impaired neurovascular coupling by transhemispheric diaschisis in rat cerebral cortex. J Cereb Blood Flow Metab 24:713–719.

Fabricius M, Lauritzen M. 1993. Transient hyperemia succeeds oligemia in the wake of cortical spreading depression. Brain Res 602:350–353.

Gold L, Lauritzen M. 2002. Neuronal deactivation explains decreased cerebellar blood flow in response to focal cerebral ischemia or suppressed neocortical function. Proc Natl Acad Sci U S A 99:7699–7704.

Hoffmeyer HW, Enager P, Thomsen KJ, Lauritzen MJ. 2007. Nonlinear neurovascular coupling in rat sensory cortex by activation of transcallosal fibers. J Cereb Blood Flow Metab 27:575–587.

Hudetz AG. 1997. Blood flow in the cerebral capillary network: a review emphasizing observations with intravital microscopy. Microcirculation 4:233–252.

Hutchinson EB, Stefanovic B, Koretsky AP, Silva AC. 2006. Spatial flow-volume dissociation of the cerebral microcirculatory response to mild hypercapnia. Neuroimage 32:520–530.

Itoh Y, Suzuki N. 2012. Control of brain capillary blood flow. J Cereb Blood Flow Metab 32:1167–1176.

Kocher M. 1990. Metabolic and hemodynamic activation of postischemic rat brain by cortical spreading depression. J Cereb Blood Flow Metab 10:564–571.

Lauritzen M. 2001. Cortical spreading depression in migraine. Cephalalgia 21:757–760.

Lauritzen M, Jorgensen MB, Diemer NH, Gjedde A, Hansen AJ. 1982. Persistent oligemia of rat cerebral cortex in the wake of spreading depression. Ann Neurol 12:469–474.

Leão A. 1944. Spreading depression of activity in cerebral cortex. J Neurophysiol 7:359–390.

Mayevsky A, Weiss HR. 1991. Cerebral blood flow and oxygen consumption in cortical spreading depression. J Cereb Blood Flow Metab 11:829–836.

Olesen J, Larsen B, Lauritzen M. 1981. Focal hyperemia followed by spreading oligemia and impaired activation of rCBF in classic migraine. Ann Neurol 9:344–352.

Olesen J, Friberg L, Olsen TS, Iversen HK, Lassen NA, Andersen AR, Karle A. 1990. Timing and topography of cerebral blood flow, aura, and headache during migraine attacks. Ann Neurol 28:791–798.

Osada T, Tomita M, Suzuki N. 2006. Spindle-shaped constriction and propagated dilation of arterioles during cortical spreading depression. Neuroreport 17:1365–1368.

Schiszler I, Takeda H, Tomita M, Tomita Y, Osada T, Unekawa M, Tanahashi N, Suzuki N. 2005. Software (KEIO-IS2) for automatically tracking red blood cells (RBCs) with calculation of individual RBC velocities in single capillaries of rat brain. J Cereb Blood Flow Metab 25(Suppl):S541.

Seylaz J, Charbonné R, Nanri K, Von Euw D, Borredon J, Kacem K, Méric P, Pinard E. 1999. Dynamic in vivo measurement of erythrocyte velocity and flow in capillaries and of microvessel diameter in the rat brain by confocal laser microscopy. J Cereb Blood Flow Metab 19:863–870.

Takano T, Tian GF, Peng W, Lou N, Lovatt D, Hansen AJ, Kasischke KA, Nedergaard M. 2007. Cortical spreading depression causes and coincides with tissue hypoxia. Nat Neurosci 10:754–762.

Tomita M, Schiszler I, Tomita Y, Tanahashi N, Takeda H, Osada T, Suzuki N. 2005. Initial oligemia with capillary flow stop followed by hyperemia during K^+-induced cortical spreading depression in rats. J Cereb Blood Flow Metab 25:742–747.

Tomita M, Osada T, Schiszler I, Tomita Y, Unekawa M, Toriumi H, Tanahashi N, Suzuki N. 2008. Automated method for tracking vast numbers of FITC-labeled RBCs in microvessels of rat brain in vivo using a high-speed confocal microscope system. Microcirculation 15:163–174.

Tomita M, Osada T, Unekawa M, Tomita Y, Toriumi H, Suzuki N. 2009. Exogenous nitric oxide increases microflow but decreases RBC attendance in single capillaries in rat cerebral cortex. Microvasc Rev Commun 3:11–16.

Tomita M, Tomita Y, Unekawa M, Toriumi H, Suzuki N. 2011. Oscillating neuro-capillary coupling during cortical spreading depression as observed by tracking of FITC-labeled RBCs in single capillaries. Neuroimage 56:1001–1010.

Unekawa M, Tomita M, Osada T, Tomita Y, Toriumi H, Tatarishvili J, Suzuki N. 2008. Frequency distribution function of red blood cell velocities in single capillaries of the rat cerebral cortex using intravital laser-scanning confocal microscopy with high-speed camera. Asian Biomed 2:203–218.

Unekawa M, Tomita M, Tomita Y, Toriumi H, Suzuki N. 2012. Sustained decrease and remarkable increase of red blood cell velocity in intraparenchymal capillaries associated with potassium-induced cortical spreading depression in rats. Microcirculation 19:166–174.

Williams JL, Shea M, Jones SC. 1993. Evidence that heterogeneity of cerebral blood flow does not involve vascular recruitment. Am J Physiol 264:H1740–H1743.

Yemisci M, Gursoy-Ozdemir Y, Vural A, Can A, Topalkara K, Dalkara T. 2009. Pericyte contraction induced by oxidative-nitrative stress impairs capillary reflow despite successful opening of an occluded cerebral artery. Nat Med 15:1031–1037.

Zhou N, Gordon GR, Feighan D, MacVicar BA. 2010. Transient swelling, acidification, and mitochondrial depolarization occurs in neurons but not astrocytes during spreading depression. Cereb Cortex 20:2614–2624.

PAIN RESEARCH 28 (2013) 167–176

Original Article

Effects of electroacupuncture on mustard oil–induced orofacial pain in rats

Shingo Saito[1,2], Kazunori Itoh[2], and Hiroshi Kitakoji[2]

[1]Graduate School of Acupuncture and Moxibustion, Meiji University of Integrative Medicine
[2]Department of Clinical Acupuncture and Moxibustion, Meiji University of Integrative Medicine

Abstract

Objects: It has been found that the orofacial region exhibits a great deal of referred pain. Substantial chronic pain results from the inability to identify the primary cause of pain. In acupuncture therapy, when the primary cause is not found, treatment to hands or feet is used for orofacial pain in addition to topical treatments. However, many questions remain regarding the therapeutic mechanism. Therefore, we examined the effects of electroacupuncture (EA) on mustard oil–induced orofacial pain in rats and also characterized the effects of naloxone in this model.

Methods: A total of 39 adult male Sprague Dawley rats (250 – 400 g) were randomized into three groups: a control [CONT] group, an EA group, and an EA + naloxone [NAL] group. Activity was recorded from functionally identified single nociceptive neurons in the trigeminal subnucleus caudalis for which mechanoreceptive fields [RFs], mechanical activation thresholds, and responses to noxious stimuli were tested in anesthetized rats. Ten minutes after 5% mustard oil (MO) injection into the masseter muscle, EA and NAL group rats received 2 Hz EA for 15 min. NAL group rats were injected with naloxone intravenously 5 min before the MO injection.

Results: In the CONT group, RFs and responses were significantly increased and the mechanical activation thresholds were deceased within 35 min of MO injection, and then gradually returned to baseline. In the EA group, however, the RFs, responses, and thresholds recovered to baseline soon after EA. In the NAL group, the time-course of RFs, responses, and thresholds were similar to those of the CONT group.

Conclusion: The results suggest that EA is effective in reducing MO-induced orofacial pain via activation of the endogenous opioid system.

Keywords
Electroacupuncture; Opioid; Orofacial pain; Referred pain; Mustard oil

Received: 11 July 2013
Accepted: 29 August 2013

咬筋へのマスタードオイル投与により引き起こされた口腔顔面痛に対する鍼通電の効果

齊藤 真吾[1,2]／伊藤 和憲[2]／北小路 博司[2]

[1]明治国際医療大学 大学院鍼灸学研究科 臨床鍼灸医学分野
[2]明治国際医療大学 鍼灸学部 臨床鍼灸学講座

はじめに

口腔顔面領域の痛みは，原因となる部位と実際に痛みを感じている部位が異なる異所性疼痛が多く，臨床的に問題となっている[17]。そのため，様々な動物モデルを用いてそのメカニズムが検討されており，その原因として解剖学的に1次ニューロンが三叉神経脊髄路核尾側亜核(Vc)に収束していることや，2次ニューロンの感作などが指摘されている[4,6]。特に2次ニューロンレベルの感作が長期化すれば慢性痛に発展することが考えられることから，初期の段階で痛みを止めることが重要となる。

一方，口腔顔面領域の痛みに対する鍼灸治療では，痛みのある局所だけでなく，手足などの遠隔部などにも治療が行われている[14]。特に，異所性疼痛のように痛みの原因が不明確な場合は，遠隔部に治療を行うことが多い。実際に，正常動物を用いた研究では，手足への鍼刺激により開口反射が抑制されたり，三叉神経脊髄路核尾側亜核（Vc）でのFos蛋白の増加が抑制されることなどが報告されており，遠隔部への鍼刺激が口腔顔面領域の痛みに対して有効であることが証明されているが[7,16]，病態モデルを用いて検討した報告は少ない。そこで今回，咬筋にマスタードオイル（以下MO）を投与することで生じたニューロンの反応変化に対して，下肢に鍼刺激をした際の効果とその作用機序を検討した。

方　法

1. 対象

実験には，SD系雄性ラットn=39（250 g～400 g）を用い，コントロール群（CONT群，n=12），鍼通電群(EA群，n=14)，鍼通電＋ナロキソン群(NAL群，n=13)の3群に無作為に群分けした。なお，本実験は明治国際医療大学研究倫理委員会の承認(23－11)を得て行った。

2. ニューロン活動の測定方法

ウレタン麻酔下(ウレタン1 g/kg・αクロロース50 mg/kg)にて静脈・動脈・気管のカニュレーションを行い，バイタルをモニターしながら延髄を露出させた後，ウレタン(0.2 g/ml)/パンクロニウム（1 mg/ml）の混合液を連続的に投与し，気管には人工呼吸器（SN-480, シナノ製作所, 東京)を接続した。

その後，Pontamine Sky Blue (2%, 0.5 M 酢酸

ナトリウム：PSB)を補填したガラス管微小電極(8～12 MΩ) を左の延髄三叉神経脊髄路核尾側亜核に刺入することでニューロン活動を記録し，触（ブラシ）あるいは圧（ウッドスティック）刺激することで，受容野の同定を行った。ニューロン活動は，プリアンプ(DAM80, WPI, USA)を介しオシロスコープ(VC-11, 日本光電, 東京）でモニターした後，A/D コンバーター(CED1401, CED, UK)を介してコンピューターに記録を行った。なお，今回の実験ではニューロンを安定して継続的に記録するために深層部のニューロンをターゲットとしたため，最初に表面から 400 μm 刺入した後，実験を開始した。

3. ニューロンの特定方法

左の顔面部の受容野に対して，ブラシによる触刺激，ウッドスティックによる圧刺激，ピンセットによるピンチ刺激を行った際のニューロンの反応特性を確認した後，強い圧やピンチにのみ反応した特異的侵害受容ニューロン(Nociceptive specific neuron：NS ニューロン)のみを実験に用いた。

4. ニューロンの反応性の評価方法

(1) ニューロンが発火する皮膚領域(受容野)の測定

ラットの顔面部の皮膚を外側からピンセットで挟み，ニューロンが発火する皮膚領域を測定し，受容野とした。なお，その受容野の範囲は，トレーシングペーパーにトレース後，画像解析ソフト(ImageJ, NIH)にて定量化した。

(2) ニューロンの発火閾値の測定

受容野を決定後，受容野の中で，定量的なピンチ刺激を加えた際にニューロンが最も発火する部位にデジタルピンセット(Pinch Meter PM-1, HI-TEQ, 東京）で圧を加え，ニューロンが発火する閾値を測定した。

(3) 定量刺激を与えた際のニューロンの発火数の測定

各ニューロンで測定した発火閾値の 1.5 倍の圧で 5 秒間圧迫した際のニューロンの発火数を記録し，オフラインで Spike2 (CED, UK) を用いてスパイク数をカウントした。

5. 病態モデルの作成

全てのラットは，受容野・発火閾値・発火数を測定した後，Hu らの報告[4] を参考に，5% MO（ナカライテスク, 京都）5 μl をマイクロシリンジ（MS-N25, 伊藤製作所, 静岡）にて口外(受容野より外)から咬筋の奥にある下顎枝周囲まで針を刺入し，1～2 mm 程度引いて左咬筋深部に投与した。

6. 鍼通電方法

EA 群と NAL 群に対して，直径 0.18 mm・長さ 40 mm のステンレス鍼 (SEIRIN, 静岡) を左の腓腹筋部 2 ヵ所(同側のみ)に刺入し，電気刺激装置 (SEN-3301, 日本光電, 東京) およびアイソレーター (SS-104JO, 日本光電, 東京) を用いて鍼通電を行った。なお，電気刺激条件は，2 Hz (パルス幅 100 μs) とし，刺激強度は筋肉が軽く収縮する程度し，MO 投与 10 分後から 15 分間鍼通電を行った。

7. 使用薬物

ナロキソン(SIGMA, USA)は，生理食塩水に溶解し，MO 投与 5 分前に静脈 (2.0 mg/kg) より投与した。

8. 実験プロトコール

全ラットは，MO 投与前，投与 5 分・10 分・

25分・35分・45分・55分後に，受容野，発火閾値，発火数をそれぞれの順番で測定した。

9. 記録部位の組織学的検討

記録部位は，実験終了後にガラス管微小電極に補填したPSBでマーキング（2 μA × 30 min）した。その後，生理食塩水と10%ホルマリン緩衝液で灌流固定した後に延髄を摘出し，マイクロスライサー（DTK-1000, 堂阪EM, 京都）で50～100 μmにスライスした切片を作成し，Crysyl Violetにて染色，記録部位を同定した。

10. 統計解析

各測定時の値はMO投与前の値を100とした時の変化率で算出し，平均±標準偏差（mean ± S.D.）で表示した。

統計処理にはStatView Version 5.0（SAS Institute Inc.）を使用し，群内比較に関してはDunnet検定で，各群間の比較は曲線下面積（Area under the curve: AUC）を算出し，F検定が有意となった場合は，さらにScheffe多重比較による検定を行った。なお，危険率5%未満を有意差ありとした。

結　果

今回は1匹から1ニューロンを記録することとし，記録できたNSニューロンは合計39ニューロンで，その内訳はCONT群で12ニューロン，EA群で14ニューロン，NAL群で13ニューロンであった。しかし，実験中ニューロンが安定しなかったり，途中記録ができなくなったケースが，CONT群で3ニューロン，EA群で5ニューロン，NAL群で4ニューロンあったため，最終的に解析に用いたニューロンは各群9ニューロン，合計27ニューロンであった。

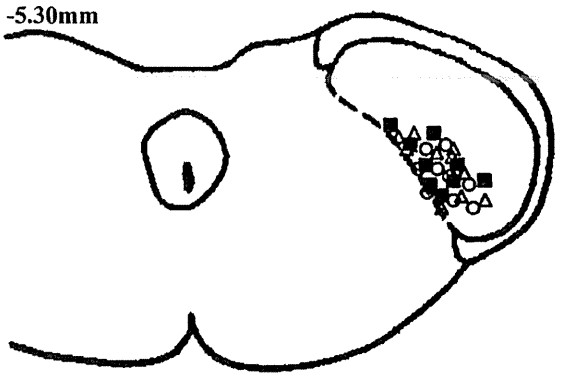

Fig.1 Histologically confirmed neuronal recording sites in subnucleus caudalis.

The sites were plotted onto a section of subnucleus caudalis (–5.30 mm behind interaural line). Twenty-seven functionally identified NS neurons were studied.

○: CONT (n=9), △: EA (n=9), ■: NAL (n=9)

1. 組織学的な解析

解析に用いた27ニューロンの記録部位を組織学的に検討したところ，ニューロンの記録部位は延髄の三叉神経脊髄路核尾側亜核の深層部で記録されたものが多かった（Fig.1）。

2. 今回記録されたニューロンの特徴

受容野はパッド周囲に記録される例が多く，その面積はCONT群で7062 ± 1943（arbitrary unit: AU），EA群で8116 ± 1399 AU，NAL群で7912 ± 1974 AUであった。また，ピンチによるニューロンの発火閾値はCONT群で37 ± 4 kg，EA群で34 ± 3 kg，NAL群では37 ± 4 kg，定量刺激を与えた際のニューロンの発火数は

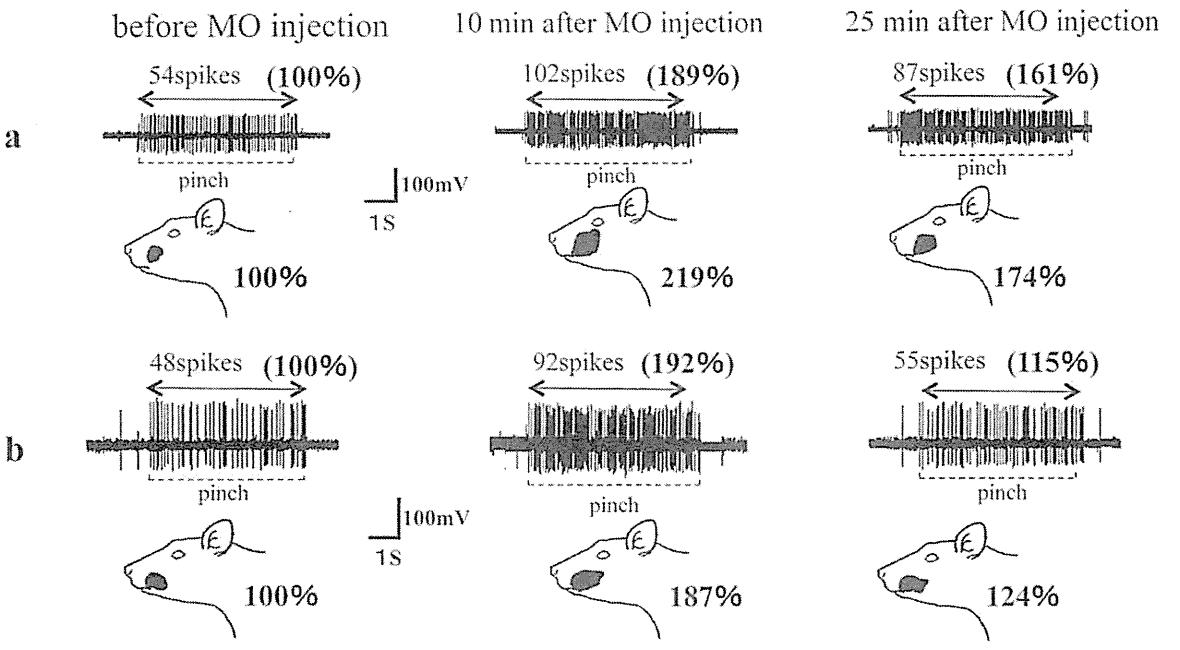

Fig.2 Representative responses to noxious stimuli and mechanoreceptive fields [RFs] with (b) and without (a) EA are shown.

Number of spikes and the area of RFs are increased after 10 minutes of MO injection and maintained at 25 minutes after injection in the subject without EA, while those with EA showed recovery to the equivalent level of the baseline.

●: RFs

CONT 群で 65 ± 22 発，EA 群で 61 ± 13 発，NAL 群で 56 ± 15 発であり，いずれも群間に差は認められなかった (Scheffe 多重比較) (Fig.2)。

一方，MO 投与後に自発性の反応が認められたニューロンは，CONT 群で 1 ニューロン，鍼通電群で 2 ニューロン，鍼通電 + ナロキソン群で 1 ニューロン存在したが，MO 投与後 1〜3 分程度で自発性の反応は観察されなくなり，MO 投与 5 分後には完全に消失していた。

3. MO投与後の受容野の変化

CONT 群では MO 投与 5 分後から眼や頭部に受容野が拡大し，10 分後には 179 ± 38% となり，35 分後まで受容野の拡大 (164 ± 31%) が認められた ($p<0.01$)。一方，EA 群では鍼通電前までは CONT 群と同様に拡大が認められたが，通電後には減少 (120 ± 18%) した。NAL 群では，EA 群で鍼通電後に認められた受容野の減少は消失し，CONT 群と同様な時間経過を辿った (Fig.3-a)。なお，群間比較において EA 群は，CONT 群と NAL 群と比較して有意差 ($p<0.05$) が認められた (Fig.3-b)。

4. MO投与後の発火閾値の変化

CONT 群では MO 投与 5 分後から発火閾値が低下し，10 分後には 65 ± 9% となり，35 分後まで閾値の低下 (66 ± 9%) が認められた ($p<0.01$)。一方，EA 群では鍼通電前までは

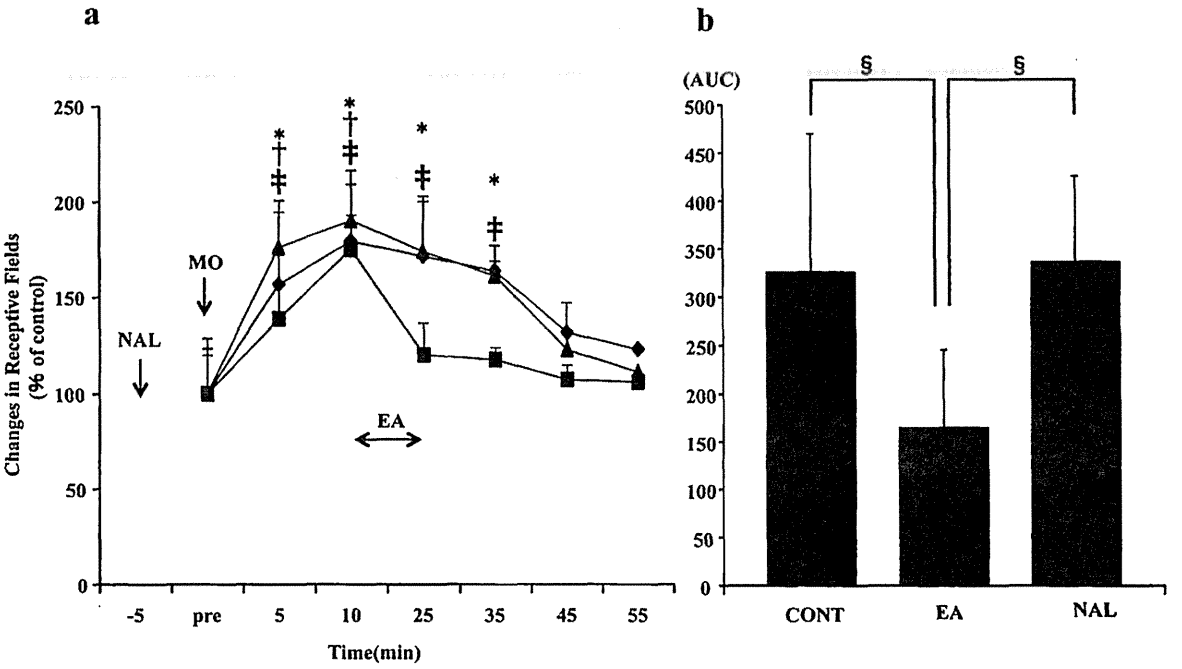

Fig.3 Changes in mechanoreceptive fields [RFs] (a) and the mean corresponding area under the RFs-time curve (AUC) of each group (b).

a : The time response curve for the RFs in three groups.
In the CONT group, the RFs was increased within 5 – 10 min after MO, which was sustained for 35 min. In the EA group, the RFs was recovered to the baseline within 25 min, while in the NAL group the recovery was similar to that of the CONT group.
◆: CONT (n=9) ■: EA (n=9) ▲: NAL (n=9)
CONT : *; p<0.01, EA : †; p<0.01, NAL : ‡; p<0.01 (compared with the value before MO injection (pre): Dunnett't test)

b : Mean AUC for the time response curve for the RFs in three groups.
The EA group was significantly different compared with the CONT and NAL groups.
§ : p<0.05 (Scheffe's multiple comparison test)

CONT 群と同様の低下が認められたが，通電後には上昇 (92 ± 6%) した。また NAL 群では，EA 群で鍼通電後に認められた閾値の上昇は消失し，CONT 群と同様な時間経過を辿った (Fig.4-a)。なお，群間比較において EA 群は，CONT 群と NAL 群と比較して有意差 (p<0.05) が認められた (Fig.4-b)。

5. MO投与後の発火数の変化

CONT 群では MO 投与 5 分後から発火数が増加し，10 分後には 180 ± 34%となり，35 分後まで発火数の増加 (162 ± 36%) が認められた (p<0.01)。一方，EA 群では鍼通電前までは CONT 群と同様の増加が認められたが，通電後には減少 (116 ± 18%) した。また NAL 群では，EA 群で鍼通電後に認められた発火数の減少は消失し，CONT 群と同様な時間経過を辿った (Fig.5-a)。なお，群間比較において EA 群は，CONT 群と NAL 群と比較して有意差 (p<0.05) が認められた (Fig.5-b)。

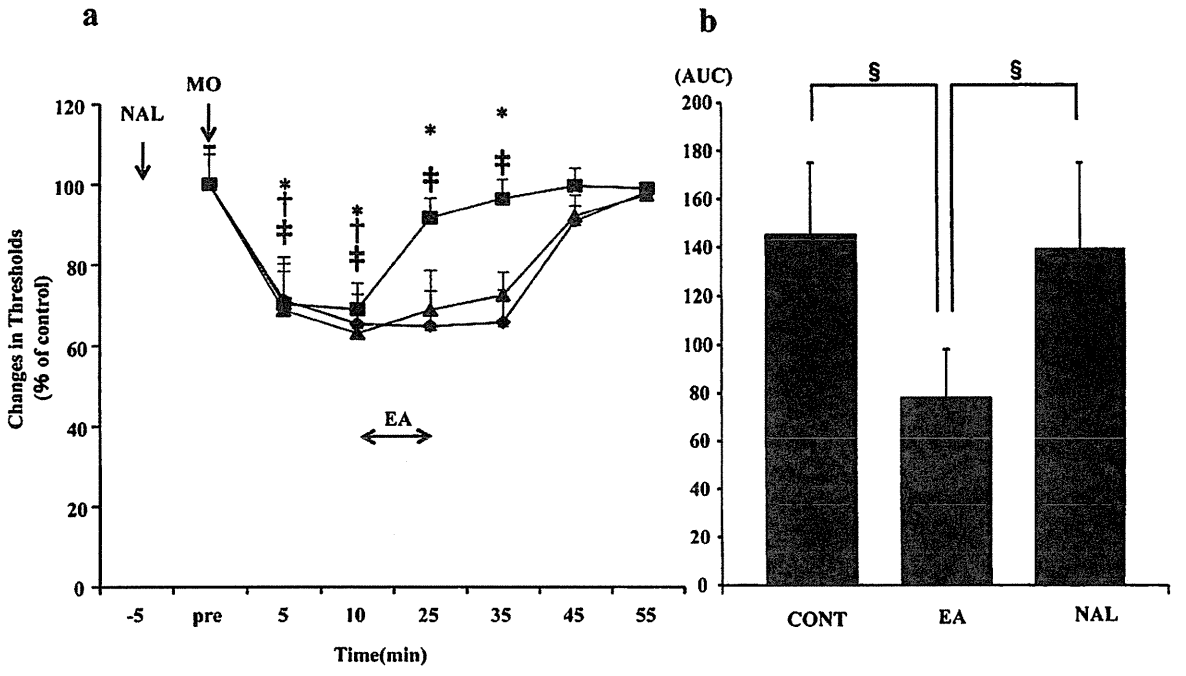

Fig.4 Changes in mechanical activation thresholds (a) and the mean corresponding area under the mechanical activation thresholds–time curve (AUC) of each group (b).

a : The time response curve for mechanical activation thresholds in three groups.
In the CONT group, Mechanical activation thresholds was decreased within 5 – 10 min after MO, which was sustained for 35 min. In the EA group, Mechanical activation thresholds was recovered to the baseline within 25 min, while in the NAL group the recovery was similar to that of the CONT group.
◆: CONT (n=9) ■: EA (n=9) ▲: NAL (n=9)
CONT : *; p<0.01, EA : †; p<0.01, NAL : ‡; p<0.01 (compared with the value before MO injection (pre): Dunnett't test)

b : Mean AUC for the time response curve for mechanical activation thresholds in three groups.
The EA group was significantly different compared with the CONT and NAL groups.
§ : p<0.05 (Scheffe's multiple comparison test)

考　察

1. 今回のモデルにおける異所性疼痛の発生機序

口腔顔面領域の異所性疼痛モデルに関しては，顎関節や咬筋などの深部組織に CFA や MO などの発痛物質を投与するモデルが多く用いられているが[4,6]，ニューロン活動を指標にした実験では疼痛のピークまでの時間が比較的短い MO モデルが多く用いられる傾向にある[4,5]。そのため，今回咬筋に MO を投与するモデルを用いたところ，5〜10 分後には皮膚ニューロンの受容野の拡大，発火閾値の低下，発火数の増加が認められ，この反応変化は 35 分程度まで確認できた。これは，Hu らの報告[4]とほぼ同様であることから，中枢の感作により異所性疼痛が出現したものと考えられる。

今回，中枢の感作の要因について詳細な検討を行っていないため，その機序は不明である

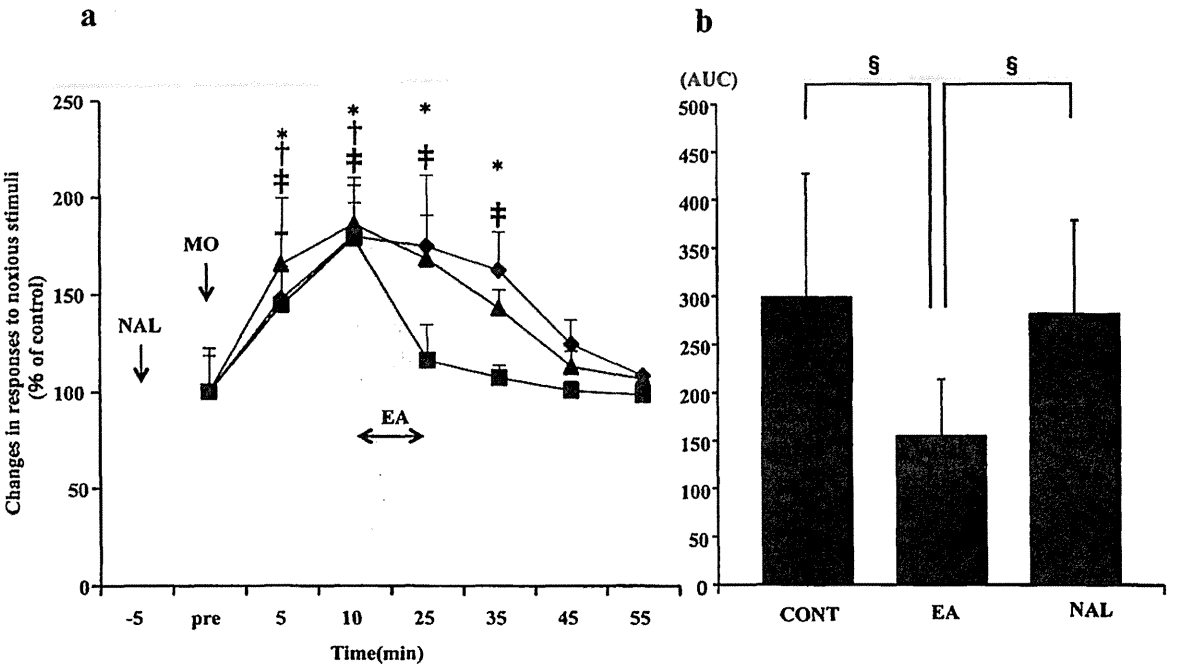

Fig.5 Changes in responses to noxious stimuli (a) and the mean corresponding area under the responses to noxious stimuli curve (AUC) of each group (b).

a : The time response curve for responses to noxious stimuli in three groups.
In the CONT group, responses to noxious stimuli was inecreased within 5 – 10 min after MO, which was sustained for 35 min. In the EA group, responses to noxious stimuli was recovered to the baseline within 25 min, while in the NAL group the recovery was similar to that of the CONT group.
◆: CONT (n=9) ■: EA (n=9) ▲: NAL (n=9)
CONT : *; p<0.01, EA : †; p<0.01, NAL : ‡; p<0.01 (compared with the value before MO injection (pre): Dunnett't test)

b : Mean AUC for the time response curve for responses to noxious stimuli was in three groups.
The EA group was significantly different compared with the CONT and NAL groups.
§ : p<0.05 (Scheffe's multiple comparison test)

が，神経障害性疼痛における中枢感作では，脊髄後角レベルにおいてニューロンの活性化，グリア細胞の活性化，脱抑制などの関与が報告されていることから[18]，今回のような侵害受容性疼痛モデルにおいても同様な機序が関与している可能性は高いものと思われる。実際，歯髄へのMO投与による侵害受容性疼痛モデルでは，脊髄後角ニューロンの活性化やグリア細胞の活性化が報告されていることから[1,5]，本モデルでも三叉神経脊髄路核尾側亜核ニューロンの活性化やグリア細胞の活性化により中枢感作が起こった可能性が高いものと考えられる。一方，脱抑制に関しては神経障害性疼痛モデル以外での検討は少ないため，本モデルのような侵害受容性疼痛モデルでも脱抑制が関与しているかは不明である。しかしながら，脱抑制は神経損傷1〜2週間後に生じることが報告されているが[2]，今回のモデルではMO投与5〜10分後にニューロンの反応性が変化したことから，脱抑制の可能性は低いものと考えられる。

2. ニューロンの反応変化に対する鍼通電の効果

今回，咬筋にMOを投与することで生じた2次ニューロンの感作(中枢感作)に対して，下肢への鍼通電効果を検討した。その結果，EA群ではCONT群で認められた発火閾値の低下，受容野の拡大，発火数の増加のいずれも抑制することが可能であったことから，口腔顔面領域での異所性疼痛に対して下肢への鍼通電が有効である可能性が示唆された。また，鍼通電の機序に関しては様々な報告があるが[8]，今回の実験ではナロキソンを投与したNAL群において鍼通電の抑制効果を拮抗したことから，その効果はゲートコントロール説や広汎性侵害抑制調節(DNIC)による鎮痛機構よりも，オピオイドを介した鎮痛機構を賦活した可能性が高いと考えられた。

オピオイドを介した鍼鎮痛機構には，下行性疼痛抑制機構と内因性オピオイド系が関与することが報告されている[8]。下行性疼痛抑制機構に関しては，下肢に低頻度の鍼通電を20～30分程度行うことで，視床下部でのβエンドルフィンの増加[3]，脊髄後角でのセロトニン放出[19]，さらにはそのセロトニンによって1次ニューロンからのサブスタンスPの放出を抑制することなどが報告されており[15]，痛みが抑制されることが知られている。このことから，今回の実験においても下行性疼痛抑制機構が賦活されることで，三叉神経脊髄路核尾側亜核でセロトニンが放出され，脊髄後角ニューロンの活性化を抑制した可能性は高いものと考えられる。

一方，内因性オピオイド系に関しては，鍼通電により髄腔内でオピオイドの放出が認められることが報告されている[9]。実際，髄腔内でのオピオイドが脊髄後角ニューロンの活性化やミクログリアの活性化に影響を与える可能性が報告されていることから[11,12]，今回の実験においても内因性オピオイド系の賦活により髄腔内に放出されたオピオイドがニューロンやミクログリアの活性化に影響を与えた可能性は否定できないが，鍼刺激による検討は少なく，その詳細は不明である。以上のことから，鍼通電によりオピオイド系の鎮痛機構を賦活させることで，三叉神経脊髄路核尾側亜核ニューロンの活性化を抑え，中枢の感作を抑制したものと考えられる。

しかしながら，オピオイドに関しては，中枢だけではなく末梢血のオピオイド増加[10]や免疫細胞からのオピオイド放出も報告されていることから[13]，本研究においても1次ニューロン末梢部で鎮痛が起った可能性を完全に否定することはできず，今後さらに検討する必要があると考えられた。

なお，今回の実験ではニューロンを安定して長期間記録するために，三叉神経脊髄路核尾側亜核の中でも深層に存在する侵害受容ニューロンを対象に実験を行ったが，侵害受容ニューロンは浅層にも存在することが知られており，浅層と深層では神経入力やニューロンの反応性が異なるとの報告もあることから，これらの違いについても今後検討する必要があると思われる。

謝　辞

稿を終えるにあたり，本研究の遂行にご助言を頂きました明治国際医療大学鍼灸学部臨床鍼灸学講座 今井賢治教授，田口玲奈先生に厚く感謝致します。